

Development of assembled microchannel resonator as an alternative fabrication method of a microchannel resonator for mass sensing in flowing liquid

Cite as: Biomicrofluidics 14, 064111 (2020); doi: 10.1063/5.0032040

Submitted: 6 October 2020 · Accepted: 6 December 2020 ·

Published Online: 17 December 2020



View Online



Export Citation



CrossMark

M. A. Indianto,^{a)} M. Toda,^{b)} and T. Ono

AFFILIATIONS

Graduate School of Engineering, Tohoku University, Sendai 980-8579, Japan

^{a)}**Author to whom correspondence should be addressed:** indianto@nme.mech.tohoku.ac.jp

^{b)}**Electronic mail:** mtoda@nme.mech.tohoku.ac.jp

ABSTRACT

We propose an alternate fabrication technique of microchannel resonators based on an assembly method of three separate parts to form a microchannel resonator on a chip. The capability of the assembled microchannel resonator to detect mass is confirmed by injecting two liquids with different densities. The experimental and theoretical values of the resonator frequency shift are in agreement with each other, which confirms the consistency of the device. The noise level of the device is estimated from the Allan variance plot, so the minimum detectable mass of 230 fg after 16 s of operation is expected. By considering the time of the practical application of 1 ms, it is found that a detectable mass of around 8.51 pg is estimated, which is applicable for detecting flowing microparticles. The sub-pico to a few picogram levels of detection will be applicable for the mass analysis of flowing microparticles such as single cells and will be greatly beneficial for many fields such as chemistry, medicine, biology, and single-cell analysis.

Published under license by AIP Publishing. <https://doi.org/10.1063/5.0032040>

I. INTRODUCTION

Microchannel resonators have been developed and widely researched in recent years to measure micro/nanoparticle mass in fluids such as single cells, protein, and DNA.^{1–13} Many advancements have been made in microchannel resonators, especially using the suspended microchannel resonator (SMR), ranging from minimizing mass and density detection resolution to extending the application of the SMR.^{4–13} Despite the achievement of the SMR, an alternate fabrication technology for microchannel resonators is also one interesting topic to be explored.

Measuring the mass and density of micro/nanoparticles, especially single cells, is one important point of interest in microchannel resonator development.^{4–7} For instance, a single cell has a defense mechanism which is called apoptosis. Apoptosis, also known as programmed cell death, occurs when a cell is damaged, either by disease or by other sources. During apoptosis, shrinkage occurs in a cell and causes a change in its mass and density.^{14–18}

Detecting the mass change of a single cell can result in the early detection of disease.

The fabrication process of the assembled microchannel resonator is based on the assembly process to form a complete device.² The assembly method also means simplification of the whole fabrication process of the device. A hollow silicon structure has been reported previously.¹³ By using the assembly method, the parts of the microchannel can be fabricated separately with a common microfabrication process such as a deep reactive ion etching (RIE) and can be assembled in the final process. By assembling with the full structure of silicon, which is a base substrate in microfabrication technology, more interesting fabrication ideas can be explored. For example, by coupling the device with piezoelectric or piezoresistive material, it is possible to extract the electrical signal directly from the resonator, which simplifies the process of actual sensor application.^{11–12} Another possibility of it being a magnetic sensor for flowing microparticles is also being considered.¹⁹

In this research, the assembled microchannel resonator is evaluated by the common concept of mass measurement in flowing liquid to observe its performance as an alternate novel type of microchannel resonator. The evaluation will include its measurement repeatability by measuring the mass of different liquids and observing its noise level. Furthermore, it is hoped that the establishment of the assembled microchannel resonator as a novel type of microchannel resonator will open up new possibilities for it in the fields of biology, chemistry, medicine, and cell diagnosis.

II. EXPERIMENTAL

A. The design concept of the assembled microchannel resonator

The assembled microchannel resonator is designed following the concept of frequency change due to additional mass to the resonating body. In the case of mass measurement of a liquid, the concept of a liquid flowing inside the resonator is applied. The equation of this phenomenon is described as follows:⁴

$$f_n - \Delta f = \frac{1}{2\pi} \sqrt{\frac{k_{eff}}{m_{eff} + \alpha \Delta m}}. \quad (1)$$

The resonance frequency of a resonator (f_n) depends on its effective spring constant (k_{eff}) and its effective mass (m_{eff}). When an additional mass (Δm) enters the microchannel, the resonance frequency will be shifted (Δf). From this frequency shift, the presence of additional mass can be known. α is a numerical constant based on the geometry of the resonator. For the bridge-type resonator, the α value is about 0.38.

The assembly method is proposed in this research as a novel type of fabrication strategy for microchannel resonators. Assembly means to fabricate separate parts of the device and assemble them in the final stage of fabrication. The assembled microchannel resonator consists of three parts: a groove part, a microchannel part, and a glass part. These three parts will be assembled to form a complete device of an assembled microchannel resonator, see Fig. 1 (assembled a + b + c).

B. Fabrication of the groove part (a) and glass part (c)

Fabrication of the groove part (a) utilizes the common deep RIE process for the top and back of a silicon on insulator (SOI) wafer. The SOI wafer with a 40 μm thick silicon device layer, a 0.5 μm thick silicon dioxide layer, and a 676 μm thick silicon handling layer is used as the groove part of the device, see Fig. 1(a-1). The process contains photolithography for patterning the desired structure and is then followed by a deep RIE process to form the structure. The first deep RIE process of the 40 μm device layer on the SOI wafer is done to form the groove part microchannel structure, see Fig. 1(a-2). The second deep RIE process of the 676 μm handling layer is done to form the 200 μm valley for the vibration of the micro-tube resonator and hole for the sealing material injection, see Fig. 1(a-3). The finishing process of the groove part is done by removing the SiO₂ layer by buffered hydrogen fluoride (BHF) solution, see Fig. 1(a-4).

The glass part (c) is meant to be the top cover of the device for forming a complete microfluidic device. For the fabrication of this part, wet etching of glass and sandblasting processes are used. A glass (Tempax) with 300 μm thickness is used for the process; see Fig. 1(c-1). Wet etching is used to open the vibrational gap for the resonator. Cr-Au is deposited to form a Cr-Au mask to prevent large-side etching to the glass due to wet etching; see Fig. 1(c-2).²⁰ The solution used for the wet etching process of the glass part is a mixed solution of hydrofluoric (HF) acid and de-ionized (DI) water with a ratio of 2:1. The sandblasting process is used to form the inlet and outlet of the device. Dry film resist is used for patterning the sandblasting process; see Fig. 1(c-3).

C. Fabrication of microchannel part (b)

The microchannel part is the main challenge in this fabrication process. Fabricating a long hollow silicon channel with a high aspect ratio has never been done before. The target of fabrication is to make a 400 μm straight and long hollow channel with an inner width of 34 μm . A deep RIE process is planned to be utilized during this fabrication process. One problem to be overcome is that an effect called the micro-loading effect will occur when performing deep RIE with such a small hole, whereas the other etching part is incomparably wide.^{21–23} The etch rate of the silicon depends on the total exposed area during the etching process; this is what is called the loading effect. However, local variations in the pattern cause a different local etch rate on each pattern; this is what is known as the micro-loading effect. Due to the micro-loading effect, the patterned inner channel area will have a much smaller etching rate compared with the outside wide area of the channel. As a result, the outside area will reach the bottom height of the channel first and will start to side-etch the outer part of the channel, while the inner part of the channel is still shallow. To overcome the micro-loading effect problem, a double-channel pattern is utilized to reduce the micro-loading effect, see Fig. 2. The inner pattern and the outside pattern of the channel are set with a ratio of 1:1. These patterns create a similar etching area between the inner part of the channel and the outside part of the channel; thus, each part will have the same etching rate.

The micro-loading effect also tends to create a tapered shape of the channel, which must be avoided as much as possible to ensure a good microfluidic channel. A modification of the deep RIE process is done to avoid the creation of the tapered shape of the microchannel. By gradually changing the etching parameter in every cycle of the deep RIE process, the creation of the tapered shape can be minimized.

The complete fabrication of the microchannel is explained as follows. An SOI wafer with a 100 μm thick silicon device layer, a 1 μm thick silicon dioxide layer, and a 400 μm thick silicon handling layer is used for the fabrication; see Fig. 1(b-1). A 2 μm silicon dioxide layer is deposited on the 400 μm handling layer of the SOI wafer using the tetraethoxysilane (TEOS) chemical vapor deposition (CVD). Photolithography patterning and silicon dioxide etching using RIE are done to make an oxide mask; see Fig. 1(b-2). As explained before, a double-channel pattern is used to reduce the micro-loading effect. A modified deep RIE process is done for the high aspect ratio vertical microchannel;

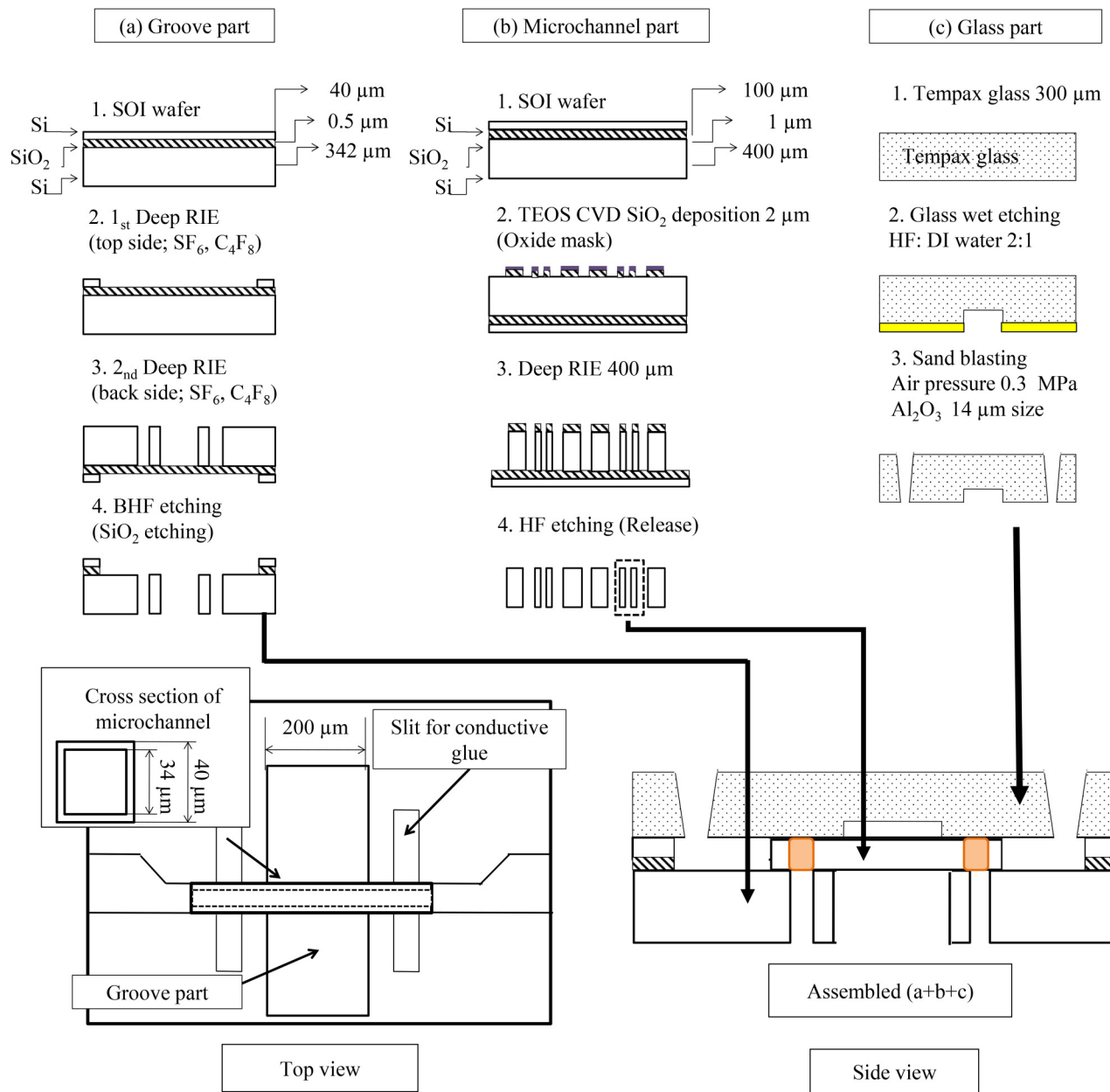


FIG. 1. Fabrication process of the assembled microchannel resonator: (a) groove part, (b) microchannel part, and (c) glass part.

see Fig. 1(b-3). For this modified deep RIE process, a three-step process in one cycle is used. Two times the etching process is followed by the deposition process of the passivation layer for the sidewall to ensure an anisotropic condition. The first etching process is to remove the passivation layer and the second etching process is to etch the silicon layer. The low frequency (LF) platen power of the first etching is set to be gradually decreasing every cycle by 0.083%. The reason for this gradual decrease is to keep

the straight line of the etched part. Continuous removal of the passivation layer might cause side etching to the microchannel wall. By gradually decreasing the LF platen power, the passivation layer can survive even in the deep etching condition and a vertical microchannel can be made. The SEM image of the double channel can be seen in Fig. 3(a). A vertical shape channel standing on the SiO₂ layer of the SOI wafer is successfully fabricated as shown in Fig. 3(b).

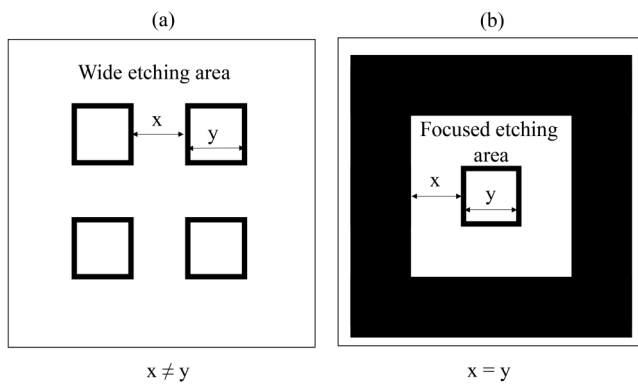


FIG. 2. Photolithography pattern of the microchannel: (a) conventional pattern and (b) double channel pattern.

To release the microchannels, a concentrated 50% HF solution has been used until all the microchannels are released from the wafer; see Fig. 1(b-4).^{24,25} The released microchannels are floating on the dangerous HF solution. To pick up the microchannels, continuous dilution of HF solution by de-ionized water is performed. This continuous dilution is meant to reduce the concentration of the HF solution to the point where it becomes safe to pick up the microchannels. A polytetrafluoroethylene filter was then used in the end to pick up all the microchannels from the diluted HF solution.

Due to the double channel pattern, not only the inner microchannel but also the outer big channel are fabricated. After the filtering process, some of the inner channels are still inside the outer channel. However, no sticking error is found and the separation process can be done easily by using a glass needle.

It is found that the bottom part of the microchannel was not completely etched during the deep RIE process while it is seen that the top side forms a hollow channel shape. An additional cut of the

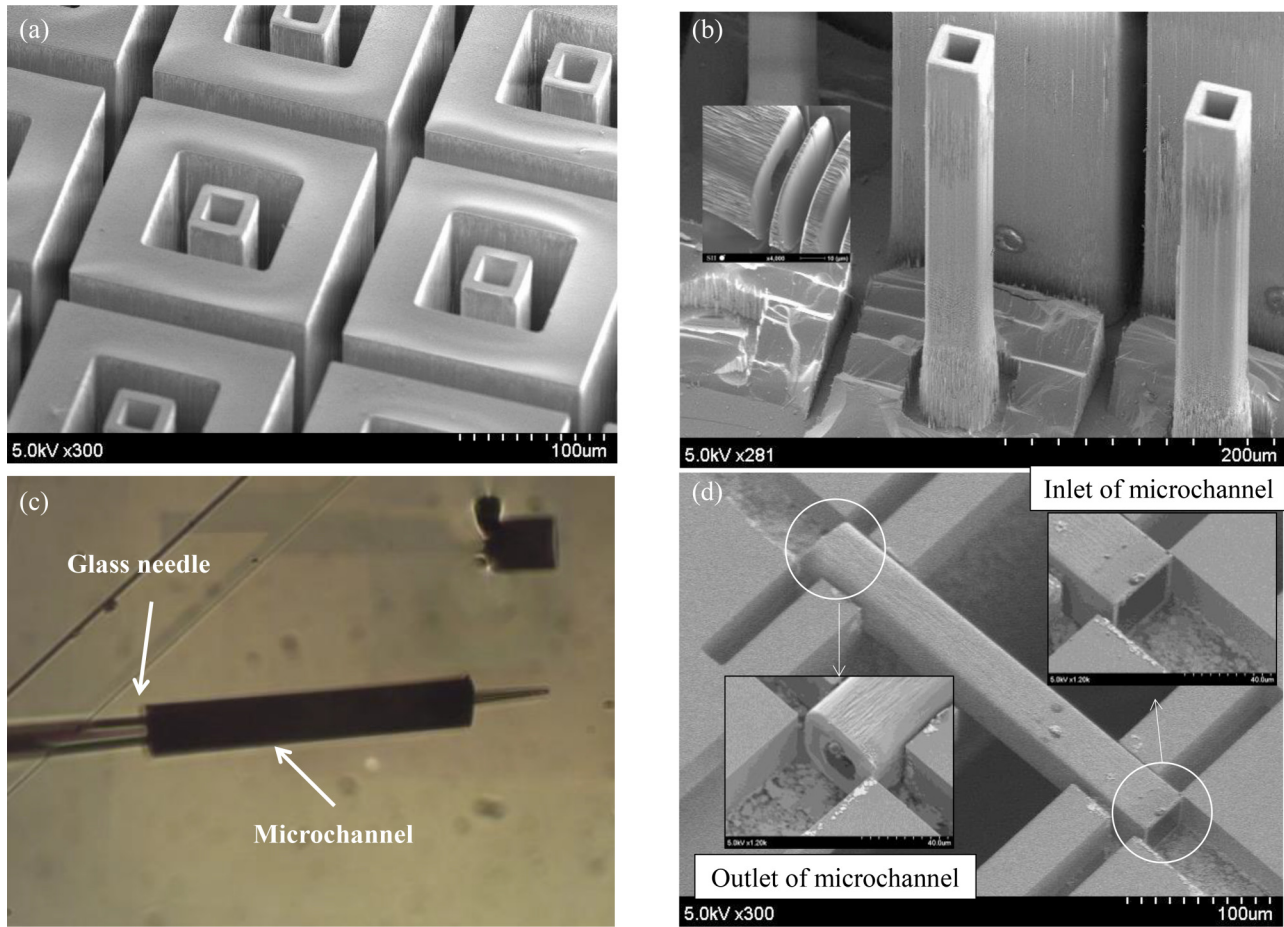


FIG. 3. Fabricated microchannel: (a) after deep RIE process using the double channel pattern, (b) fabricated part of the inside microchannel; the bottom hole is formed by FIB cut, (c) pickup process of the microchannel using a glass needle, and (d) fabricated part of the final assembled microchannel resonator.

microchannel part using a focused ion beam (FIB) has been done to open the bottom hole of the microchannel part; see Fig. 3(b). The actual length of the microchannel obtained is 330 μm ; see Fig. 3(c).

The inlet and the outlet of the microchannel are slightly different in width. The outlet side is smaller than the inlet side; see Fig. 3(c). This indicates that the inner side of the microchannel has a tapered shape due to the micro-loading effect of the deep RIE process. However, the use of a double-channel pattern followed by a modified deep RIE process proved successful in minimizing the whole taper shape of the channel and forming a microchannel. The optimized double pattern ratio might completely overcome the micro-loading effect to form a long microchannel with a complete shape.

D. Assembling the three parts

To assemble the three parts, a glass needle attached to a micromanipulator is used to place the microchannel on the groove part of the device. The fixation method used for this assembly point is by sticking a silver paste. The silver paste is first stuck using a glass needle on the surface of the groove part where the microchannel will be placed. Then using a different glass needle, the microchannel is picked up and placed on the groove part; see Fig. 2(c). The sharp tip of the glass needle can be inserted into the microchannel part. By inserting the glass needle into the microchannel, it can be transferred freely and placed on the groove part. The aligning process is done optically using a microscope. After the assembly process is completely, the microchannel is then detached from the glass needle. The assembled groove part and the microchannel part are then heated up on a hot plate to cure the silver paste and fix the assembly point. This process is then followed by an anodic bonding process with the glass part to form a complete structure of the assembled microchannel resonator; see Fig. 1 (assembled a + b + c). The anodic bonding is meant to cover the top side of the device and to be the inlet and outlet of the device.

For the sealing process, silver paste is stuck to cover the back hole of the device. This process is then followed by the vacuuming process to push the silver paste inside. The sealing process is finalized by heating up on a hot plate to cure the silver paste. The new fabricated assembled microchannel can be seen in Fig. 3(c). The length of the resonator part is 200 μm .

E. Measurement setup of the system

To evaluate the fabricated assembled microchannel resonator, two systems based on a laser Doppler vibrometer (LDV) for the resonant frequency measurement of the resonator have been used. One system is an open-loop measurement system with a lock-in amplifier. This experimental setup is to evaluate the performance of mass detection with liquid flow in the channel by detecting the peak of the resonant frequency. The second system is a closed loop with a phase-locked loop (PLL). This experimental setup is to evaluate the noise of the system. A piezoceramic actuator is used to vibrate the resonator with the actuation voltage supplied from the internal generator. The experimental setup can be seen in Fig. 4.

The resonance frequency of the assembled microchannel resonator is changed depending on the additional mass inside the microchannel. To evaluate the mass sensing capability, de-ionized (DI) water and ethanol are injected in sequence inside the

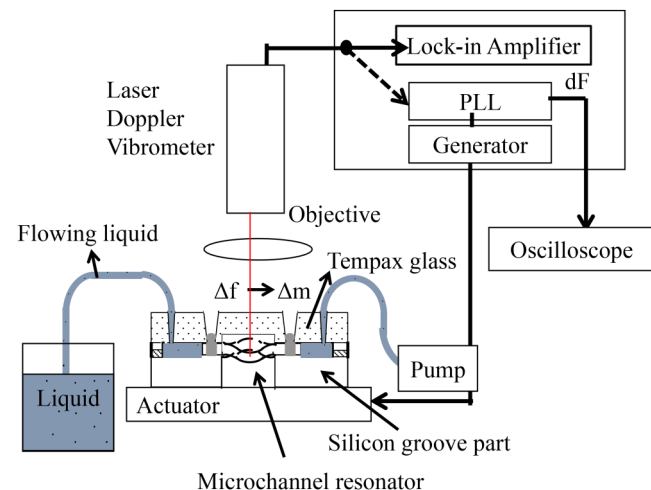


FIG. 4. Experimental setup for resonance peak and frequency stability observation.

microchannel. A change of the resonance frequency is then observed. This experimental result is compared with the theoretical value to conclude its consistency.

The second system is set up for the evaluation of the resonator's noise level. A noise analysis of this system is done by using the PLL system of the lock-in amplifier. The PLL system will compare the phase of the reference signal with an output signal whose phase is related to the reference. The deviation from the reference will be recorded as the frequency shift as its output signal. The purpose of this PLL system is to detect the noise level of the assembled microchannel resonator; therefore, the bandwidth of the PLL system is set to be 100 Hz. The output signal of the resonance frequency shift from the PLL system is connected to the oscilloscope to record the frequency stability of the system by the Allan variance analysis; see Fig. 4. An oscillator dataset contains the time-dependent noise, which is contributed by low-frequency phenomena such as natural disturbances. In the Allan variance analysis, the noise generated by the time of operation can be separated, whether it comes from the high-frequency phenomena of white noise, the noise floor flicker noise, or the random walk noise which generally comes from natural disturbances. By this analysis, controllable noise such as white noise can be determined and the means to improve the device can be determined. A more detailed explanation will be provided in the Secs. III–IV of this paper.

III. RESULTS AND DISCUSSION

A. Resonant peak observation of an assembled microchannel resonator

The initial evaluation of the device is performed with the assembled microchannel resonator with no liquid injected inside the microchannel. The assembled microchannel resonator is vibrated with the piezoceramic actuator under atmospheric pressure conditions. The resonance peak in amplitude is observed by

sweeping the actuation frequency using the LDV system. The laser position of the LDV is focused on the specific place where we want the vibration to be observed. A simulation using COMSOL is also done with the assembled microchannel design for comparison with the experimental result.

An evaluation of the assembled microchannel resonator with air inside can be seen in Fig. 5. The resonance frequency observed by the LDV is 4.55 MHz in the center part of the microchannel with the quality factor (Q factor) of 120, as seen in Fig. 5(a). This vibration is confirmed with the variation of LDV laser position and actuation voltage. It is confirmed that the vibration is dependent on the laser position and the actuation voltage, which indicates that the vibration that occurs is the true vibration of the resonator; see Fig. 5(b).

This experimental value of resonance frequency is then compared with the simulation result. The simulation result shows that the resonance frequency of the design is in the value of 7.2 MHz. One consideration of the resonance frequency difference is that the fabricated structure deviates from the design. The point that is considered to be changed is the inner channel size and the length of the resonator. The inner channel size is slightly different due to the micro-loading effect, and the length of the resonator is changed due to imperfect anodic bonding conditions. By calculation, it is determined that the actual average inner channel size is about 32.5 μm and the microchannel is fixed in the sealing hole position with a length of 312.5 μm . With this adjustment, the calculated resonance frequency is matched with the experimental value of 4.55 MHz.

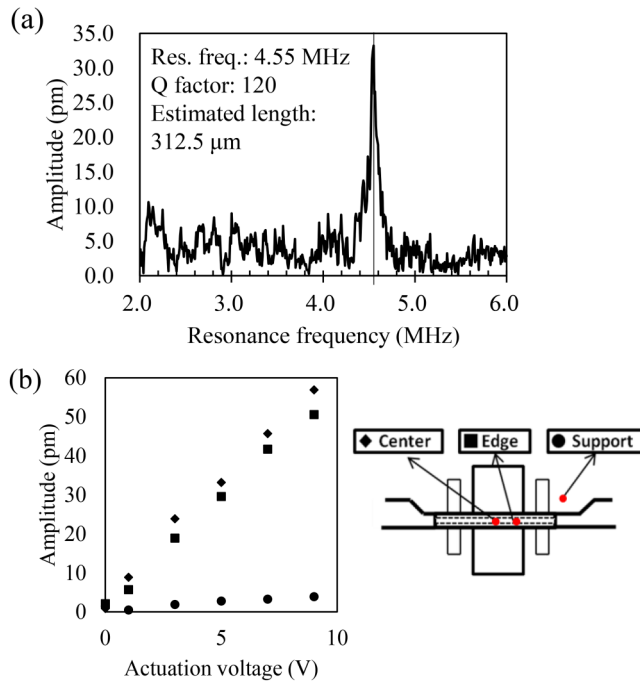


FIG. 5. (a) Peak at resonance frequency measured by LDV. (b) Actuation voltage and position dependence of the resonance peak.

B. Evaluation of mass sensing performance

Two types of liquid are injected inside the microchannel to test the mass sensing capability of the assembled microchannel resonator. The resonance frequency is observed by the LDV using the same condition used in the previous measurement. Theoretical calculations are done to see whether they are consistent with the experimental results.

An evaluation of the assembled microchannel resonator with DI water inside showed that the resonance frequency observed by the LDV is 3.37 MHz on the center part of the microchannel with a Q factor of 112. When it is injected by the 100% ethanol, the resonance frequency is observed in the value of 3.54 MHz on the center part of the microchannel with a Q factor of 119. The minimum change of the Q factor indicates minimum power loss during liquid injection to the microchannel. The mass responsivity of the device is calculated from these two results with the value of 2816.9 Hz/ng. All of these results are provided in Fig. 6(a).

These results are consistent with the theoretical calculations as plotted on the graph in Fig. 6(b). These results show a promising

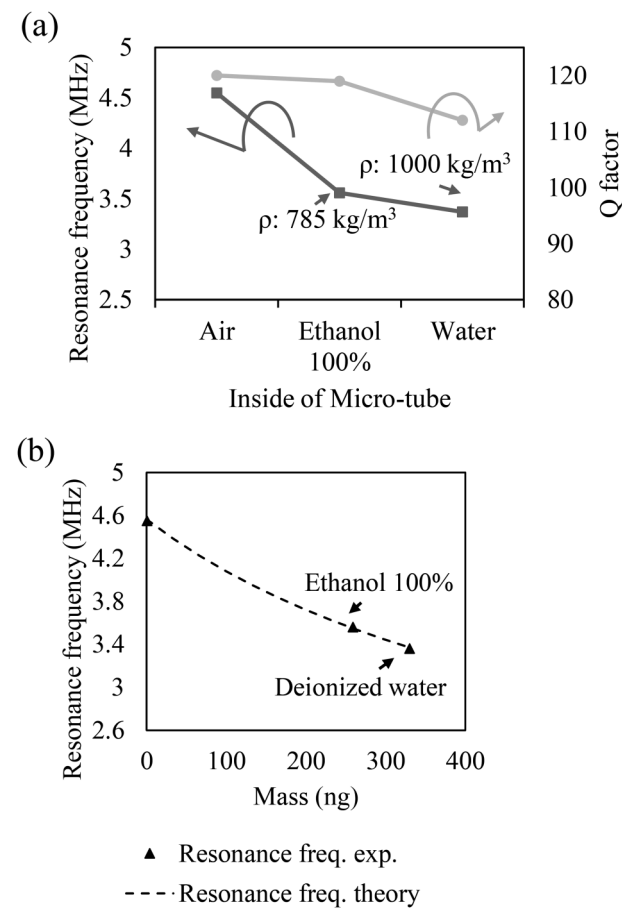


FIG. 6. (a) Comparison of resonance frequency and Q factor change of different liquids. (b) Theoretical and experimental comparison of mass change.

capability for the assembled microchannel resonator to be used as a mass sensor. As a mass sensor, further application for microparticles mass detection is expected in such a system. The system's noise level should match the requirement of mass resolution of microparticles.

C. Minimum detectable mass of the microchannel resonator

To analyze the noise level and minimum detectable mass, the Allan variance plot is utilized. As mentioned before, Allan variance is a measure of the frequency stability of an oscillator. It is defined by the following equation:^{26,27}

$$\sigma_y^2(\tau) = \frac{1}{2}((\bar{y}_{n+1} - \bar{y}_n)^2), \quad (2)$$

where σ_y^2 is the Allan variance, τ is the observation period, and \bar{y}_n is the n th fractional frequency average over the observation time τ . The fractional frequency is obtained as follows: the frequency noise signal from the PLL is divided by the resonance frequency of the resonator. Allan deviation is the square root of the Allan variance as described below:

$$\sigma_y(\tau) = \sqrt{\sigma_y^2(\tau)}. \quad (3)$$

Allan deviation analysis will enable us to know the level of frequency stability in each period. Eventually, noise floor stability will be achieved before it increases again due to noise from natural disturbances.

From the Allan variance analysis graph in Fig. 7, the minimum frequency noise is calculated by its square root and then by dividing it with the resonance frequency of the resonator. The minimum frequency noise stability of the device is 2.2 Hz after 16 s. The frequency noise is equivalent to adding mass to the

resonant body, as mentioned in Eq. (1). As per Eq. (1), 2.2 Hz of frequency shift is equivalent to 230 fg mass detection by the resonator. For the operation of flowing microparticles through the microchannel, 16 s is unpractical due to incomparable detection time and the time needed for the microparticles to pass through the microchannel. However, it is seen that in the region of 1 ms, the frequency noise is still in the value of 80 Hz which is equal to 8.51 pg mass addition to the resonator body. With the microchannel resonator's length of 200 μm and the estimated flow speed of the liquid of 10 mm/s, the time needed for the microparticles to pass through the microchannel is about 2 ms, which is still compatible with the 1 ms response time of the resonator. This result is a promising indication that the device is usable for the mass detection of flowing microparticles.

To determine whether the noise level is acceptable for micro-particle mass detection, a simple calculation has been done. One of the remaining interesting points relating to mass detection at the micro-scale level is the single-cell analysis. In this type of analysis, one of the most important phenomena is apoptosis, which is known as the cell's programmed suicide system.^{10–13} Apoptosis occurs when a cell is damaged by diseases such as viruses or other means. During apoptosis, a cell will undergo shrinkage, which will change its mass and density. Detecting such mass change is important for processes such as early detection of disease. Therefore, in this research, the possibility of detecting such a phenomenon will be one of the specifications to determine the performance of the assembled microchannel resonator.

For example, a lymphocyte with a diameter estimation of 15 μm and a density of 1073 kg/m³ is set as the target of measurement.²⁸ Estimating with simple sphere volume, we get a volume of $1.4 \times 10^4 \mu\text{m}^3$. The cell will remove water in the same volume. Thus, we will get a mass change of around 1000 pg. If we estimate when apoptosis occurs, there will be a 5–10% change of mass, and then the mass change will be around 50–100 pg. In the previously reported paper, it is also shown that during apoptosis, the mass change of pg range is needed to observe the apoptosis of a single cell.¹⁸ Comparing the value of the noise level and the target mass detection of apoptosis in a single cell, it can be concluded that with the mass resolution of the pg range, the assembled microchannel resonator is capable of detecting apoptosis in a single cell. In terms of high sensitive sensing, the assembled microchannel resonator is still far below the previously reported mass detection of the micro-channel resonator of 7 zg⁴. However, one of the purposes of this device is to fabricate a wide microchannel for the application of the single-cell analysis with a diameter of up to 20 μm . For such a purpose, the pg range of detection is applicable. Moreover, improvements can be made by considering the reduction of the noise of the system.

The reduction of the noise level is possible when the source of noise can be defined. From the Allan variance analysis in Fig. 7, the source of noise can be plotted. The noise source before the minimum stable frequency emanates from white noise. It is also known as thermal noise, which is the common main noise from the resonator.

To improve the mass detection capability of the assembled microchannel resonator, the reduction of thermal noise can be done by modifying the resonator's structure. The thermal noise is

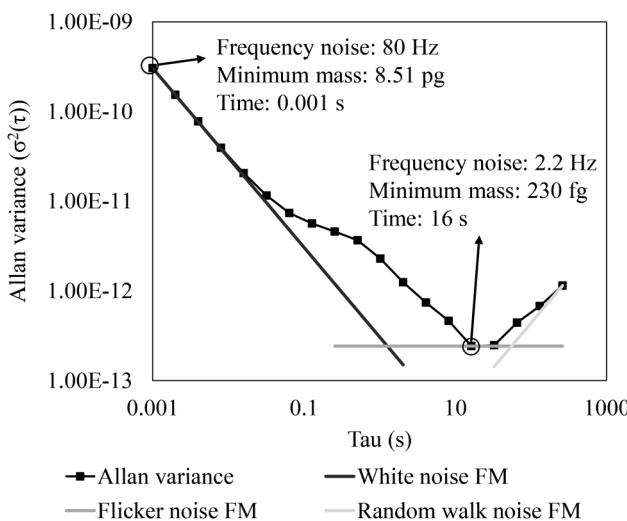


FIG. 7. Allan variance analysis of an assembled microchannel resonator.

described by the following equation:^{29,30}

$$\Delta m_{\min} \approx \frac{2Gk^{0.5}}{(\pi f_n)^{2.5}} \sqrt{\frac{k_B T B}{\tau Q(z_{osc}^2)}}, \quad (4)$$

where Δm_{\min} is the minimum detectable mass of thermal noise, G is a geometrical factor, k is the spring constant, f_n is the resonance frequency, k_B is the Boltzmann constant, T is the temperature, B is the bandwidth, τ is the time constant, Q is the quality factor, and z_{osc} is the amplitude.

From this equation, it can be seen that one important parameter is the Q factor. If the resonator can have a very high Q factor, then the minimum detectable mass can be much lower. One improvement that can be done is by using the assembly method of the assembled microchannel resonator. The current device now has a low Q factor even though it is made of silicon which usually has a high Q factor. The use of silver paste as a method of assembly might be one factor. By changing the assembly method, the Q factor of the device can be improved. One of the possibilities is by utilizing the micro-clamping method. Two research papers have reported such a method as the assembly method.^{31,32} Another way to improve the Q factor is by vacuum encapsulation as it is widely reported in the literature.^{13,26,33–39}

IV. CONCLUSIONS

The proposed assembled microchannel resonator has been fabricated and evaluated. The capability of mass detection has also been confirmed with consistent results and comparing them with theoretical calculations. A minimum detectable mass value of 8.51 pg with a measurement time of 1 ms will be applicable for measuring a flowing microparticle through the microchannel. These results show that the performance of the assembled microchannel resonator is good, and it can be used as an alternate microchannel resonator mass sensor. Further improvements to the resonator can be done by reducing its thermal noise, which is its main source of noise. Such improvements will open up its application for even more sensitive requirements.

ACKNOWLEDGMENTS

M.T. acknowledges the partial financial support provided by the Promotion of Joint International Research by the JSPS KAKENHI, Grant No. 19H02568. Part of this work was performed at the Micro/Nano machining Research and Education Center (MNC) and Micro System Integration Center (μ SIC) of Tohoku University. M.A.I. was financially supported by the Indonesia Endowment Fund for Education (LPDP) and Japan International Cooperation Agency (JICA) during the study at Tohoku University, Japan.

DATA AVAILABILITY

The data that support the findings of this study are available within the article.

REFERENCES

¹J. Lee, W. Shen, K. Payer, T. P. Burg, and S. R. Manalis, *Nano Lett.* **10**, 2537 (2010).

- ²M. A. Indianto, M. Toda, and T. Ono, in *IEEE Micro Electro Mechanical Systems* (IEEE, 2018), pp. 1261–1264.
- ³M. Godin, A. K. Bryan, T. P. Burg, K. Babcock, and S. R. Manalis, *Appl. Phys. Lett.* **91**, 123121 (2007).
- ⁴T. P. Burg, M. Godin, S. M. Knudsen, W. Shen, G. Carlson, J. S. Foster, K. Babcock, and S. R. Manalis, *Nature* **446**, 1066 (2007).
- ⁵A. K. Bryan, A. Goranov, A. Amon, and S. R. Manalis, *Proc. Natl. Acad. Sci. U.S.A.* **107**, 999 (2010).
- ⁶W. H. Grover, A. K. Bryan, M. Diez-Silva, S. Suresh, J. M. Higgins, and S. R. Manalis, *Proc. Natl. Acad. Sci. U.S.A.* **108**, 10992 (2011).
- ⁷A. K. Bryan, V. C. Hecht, W. Shen, K. Payer, W. H. Grover, and S. R. Manalis, *Lab Chip* **14**, 569 (2014).
- ⁸M. M. Modena, Y. Wang, D. Riedel, and T. P. Burg, *Lab Chip* **14**, 342 (2014).
- ⁹N. Cermak, S. Olcum, F. F. Delgado, S. C. Wasserman, K. R. Payer, M. A. Murakami, S. M. Knudsen, R. J. Kimmerling, M. M. Stevens, and Y. Kikuchi, *Nat. Biotechnol.* **34**, 1052 (2016).
- ¹⁰A. De Pastina and L. G. Villanueva, *J. Micromech. Microeng.* **30**, 43001 (2020).
- ¹¹A. De Pastina, D. Maillard, and L. G. Villanueva, *Microelectron. Eng.* **192**, 83 (2018).
- ¹²J. Lee, R. Chunara, W. Shen, K. Payer, K. Babcock, T. P. Burg, and S. R. Manalis, *Lab Chip* **11**, 645 (2011).
- ¹³T. P. Burg, A. R. Mirza, N. Milovic, C. H. Tsau, G. A. Popescu, J. S. Foster, and S. R. Manalis, *J. Microelectromech. Syst.* **15**, 1466 (2006).
- ¹⁴S. Elmore, *Toxicol. Pathol.* **35**, 495 (2007).
- ¹⁵C. D. Bortner and J. A. Cidlowski, *Biochem. Pharmacol.* **56**, 1549 (1998).
- ¹⁶S. Becila, C. H. Herrera-Mendez, G. Coulis, R. Labas, T. Astruc, B. Picard, A. Boudjellal, P. Pelissier, L. Bremaud, and A. Ouali, *Eur. Food Res. Technol.* **231**, 485 (2010).
- ¹⁷C. D. Bortner and J. A. Cidlowski, *J. Biol. Chem.* **278**, 39176 (2003).
- ¹⁸T. Vicar, M. Raudenska, J. Gumulec, and J. Balvan, *Sci. Rep.* **10**, 1 (2020).
- ¹⁹H. Lee, E. Sun, D. Ham, and R. Weissleder, *Nat. Med.* **14**, 869 (2008).
- ²⁰J.-Y. Jin, S. Yoo, J.-S. Bae, and Y.-K. Kim, *J. Micromech. Microeng.* **24**, 15003 (2013).
- ²¹J. Yeom, Y. Wu, J. C. Selby, and M. A. Shannon, *J. Vac. Sci. Technol. B* **23**, 2319 (2005).
- ²²C. Hedlund, H. Blom, and S. Berg, *J. Vac. Sci. Technol. A* **12**, 1962 (1994).
- ²³B. Wu, A. Kumar, and S. Pamarthi, *J. Appl. Phys.* **108**, 051101 (2010).
- ²⁴J. Bühl, F. P. Steiner, and H. Baltes, *J. Micromech. Microeng.* **7**, R1 (1997).
- ²⁵D. J. Monk, D. S. Soane, and R. T. Howe, *Thin Solid Films* **232**, 1 (1993).
- ²⁶B. Bahreyni, *Fabrication & Design of Resonant Microdevices* (William Andrew, 2008).
- ²⁷D. Jin, X. Li, J. Liu, G. Zuo, Y. Wang, M. Liu, and H. Yu, *J. Micromech. Microeng.* **16**, 1017 (2006).
- ²⁸A. Zipursky, E. Bow, R. S. Seshadri, and E. J. Brown, *Blood* **48**, 361–371 (1976).
- ²⁹T. Ono, D. F. Wang, and M. Esashi, in *Sensors*, (IEEE, 2003), pp. 825–829.
- ³⁰Y.-J. Seo, M. Toda, and T. Ono, *J. Micromech. Microeng.* **25**, 45015 (2015).
- ³¹K. Kotani, Y. Kawai, C.-Y. Shao, and T. Ono, in *2011 IEEE 24th International Conference on Micro Electro Mechanical Systems* (IEEE, 2011), pp. 209–212.
- ³²Y. Kawai, K. Kotani, C.-Y. Shao, and T. Ono, *IEEE Trans. Sens. Micromachines* **135**, 98 (2015).
- ³³B. Lee, S. Seok, and K. Chun, *J. Micromech. Microeng.* **13**, 663 (2003).
- ³⁴H. Henmi, S. Shoji, Y. Shoji, K. Yoshimi, and M. Esashi, *Sens. Actuators A* **43**, 243 (1994).
- ³⁵A. Hilton and D. S. Temple, *Sensors* **16**, 1819 (2016).
- ³⁶N. Mohd, G. Xue, N. Inomata, N. Van Toan, M. Toda, and T. Ono, *IEEE Trans. Sens. Micromachines* **137**, 245 (2017).
- ³⁷G. Xue, M. Toda, and T. Ono, in *19th International Conference on Solid-State Sensors, Actuators and Microsystems* (IEEE, 2017), pp. 1096–1099.
- ³⁸M. S. Al Farisi, H. Hirano, and S. Tanaka, *Sens. Actuators A* **279**, 671 (2018).
- ³⁹M. S. Al Farisi, H. Hirano, J. Frömel, and S. Tanaka, *J. Micromech. Microeng.* **27**, 15029 (2016).